AFRL-RW-EG-TP-2008-7416

SUPERSONIC PENETRATION BY WEDGES AND CONES INTO DRY SAND (PREPRINT)

William J. Flis
David Jann
Lucia Shan
DE Technologies, Inc.
100 Queens Drive
King of Prussia, PA 19406

JUNE 2008

CONFERENCE PAPER PREPRINT

This paper was submitted for presentation to the 24th International Symposium on Ballistics to be held in September 22-26 2008 in New Orleans, LA. If presented, it will be published in the proceedings. If this work is published, the National Defense Industrial Association may assert copyright. This work was funded in whole or in part by the Department of the Air Force contract number FA8651-05-C-0114.

This paper is published in the interest of the scientific and technical information exchange. Publication of this paper does not constitute approval or disapproval of the ideas or findings.

AIR FORCE RESEARCH LABORATORY, MUNITIONS DIRECTORATE

■ **Air Force Materiel Command** ■ **United States Air Force** ■ **Eglin Air Force Base**

REPORT DOCUMENTATION PAGE	Form Approved OMB No. 0704-0188

PLEASE DO NOT RETURN YOUR FORM TO THE ABOVE ADDRESS.

1. REPORT DATE *(DD-MM-YYYY)*	2. REPORT TYPE	3. DATES COVERED *(From - To)*
06-2008	CONFERENCE PAPER (PREPRINT)	

4. TITLE AND SUBTITLE

SUPERSONIC PENETRATION BY WEDGES AND CONES INTO DRY SAND

5a. CONTRACT NUMBER

FA8651-05-C-0114

5b. GRANT NUMBER

N/A

5c. PROGRAM ELEMENT NUMBER

65502F

6. AUTHOR(S)

William J. Flis
David Jann
Lucia Shan

5d. PROJECT NUMBER

3005

5e. TASK NUMBER

45

5f. WORK UNIT NUMBER

43

7. PERFORMING ORGANIZATION NAME(S) AND ADDRESS(ES)

DE Technologies, Inc.
100 Queens Drive
King of Prussia, PA 19406

8. PERFORMING ORGANIZATION REPORT NUMBER

AFRL-RW-EG-TP-2008-7416

9. SPONSORING/MONITORING AGENCY NAME(S) AND ADDRESS(ES)

Air Force Research Laboratory
Munitions Directorate
AFRL/RWAC
Eglin AFB, FL 32542-6810

10. SPONSOR/MONITOR'S ACRONYM(S)

AFRL-RW-EG

11. SPONSOR/MONITOR'S REPORT NUMBER(S)

SAME AS BLOCK 8

12. DISTRIBUTION/AVAILABILITY STATEMENT

DISTRIBUTION A: Approved for public release; distribution unlimited.
Approval Confirmation 96 ABW/PA # 06-05-08-285; dated 5 June 2008.

13. SUPPLEMENTARY NOTES

CONFERENCE PAPER PREPRINT See 'cover page' for pertinent metadata information.

14. ABSTRACT

An analytical model of penetration by non-deforming pointy projectiles into dry sand is proposed. The model postulates that an oblique compaction wave in the sand is attached to the penetrator's tip. Sand is modeled by the P-α porosity model up to full compaction, then is taken as incompressible. The sand's compaction is considered the most important effect; strength and friction are neglected. The model handles wedges, for which a closed-form solution is derived, and cones, which require numerical integration. For a given penetration velocity, the model predicts the shock angle and the pressure on the penetrator surface. Hydrocode computations agree closely with the model.

15. SUBJECT TERMS

Not provided.

16. SECURITY CLASSIFICATION OF:			17. LIMITATION OF ABSTRACT	18. NUMBER OF PAGES	19a. NAME OF RESPONSIBLE PERSON
a. REPORT	b. ABSTRACT	c. THIS PAGE			YEN TU
UNCLASSIFIED	UNCLASSIFIED	UNCLASSIFIED	SAR	10	19b. TELEPHONE NUMBER *(Include area code)*

24th International Symposium on Ballistics
New Orleans, Louisiana, 22-26 September 2008

SUPERSONIC PENETRATION BY WEDGES AND CONES INTO DRY SAND

William J. Flis, David Jann, and Lucia Shan
DE Technologies, Inc., 100 Queens Drive, King of Prussia, PA 19406

An analytical model of penetration by non-deforming pointy projectiles into dry sand is proposed. The model postulates that an oblique compaction wave in the sand is attached to the penetrator's tip. Sand is modeled by the P-α porosity model up to full compaction, then is taken as incompressible. The sand's compaction is considered the most important effect; strength and friction are neglected. The model handles wedges, for which a closed-form solution is derived, and cones, which require numerical integration. For a given penetration velocity, the model predicts the shock angle and the pressure on the penetrator surface. Hydrocode computations agree closely with the model.

INTRODUCTION

An analytical model of penetration in dry sand by sharp conical-nosed penetrators is proposed. The model predicates the existence in the sand of an oblique compaction shock attached to the nose of the penetrator, which is pointy: a wedge in plane flow or a cone in axisymmetric flow. The penetrator's deceleration is assumed too slow to affect the flow, so from its point of view the sand flows steadily around it. Sand, with its intergranular voids, is modeled by the P-α compaction model[1]; for a shock to form, the flow must be supersonic.

A compaction shock stands as an oblique wave attached to the penetrator apex. The spaces between the sand grains are assumed to be at least partially crushed out in this wave. For wedge penetrators, the sand is deflected within the shock by an angle equal to the wedge angle; that is, the sand flows parallel to the wedge surface (and with no further compaction). For cones, the shock deflects the sand by an angle smaller than the apex angle, and the subsequent flow follows a curved path that asymptotically approaches the cone surface, with further compaction.

MODEL DEVELOPMENT

The compaction behavior of the sand is described by the P-α model, Fig. 1, given by

$$\alpha = \begin{cases} 1 + (\alpha_0 - 1)\left[\dfrac{P_s - P}{P_s}\right]^2 & \text{for} \quad P < P_s \\ 1 & \text{for} \quad P \geq P_s \end{cases} \tag{1}$$

where α is a porosity parameter (with initial value $\alpha_0 > 1$), $\alpha \equiv \rho_s/\rho$, in which ρ is the current density, ρ_s the fully compacted density, and P_s the pressure at complete compaction. Parameters established for dry sand[2] are used: as pressure increases, the sand is gradually crushed from an initial density of 1.6 g/cm^3 to 2.65 g/cm^3 ($\alpha_0 = 1.66$) at a pressure P_s of 250 MPa.

Distribution A: Approved for public release; distribution unlimited. Approval Confirmation #96 ABW/PA-06-05-08-285. This work was funded in whole or in part by Department of the Air Force Contract #FA8651-05-C-0114.

Once compaction is complete, the material is assumed in this model to behave incompressibly (but in the hydrocode computations, fully compacted sand is modeled as quartz).

Suddenly compressing a porous material creates a compaction wave, behind which some or all of the porosity has been crushed out, depending on the loading. The wave is actually a shock, across which the material incurs sudden changes in velocity, density, and pressure, as described by the same equations as govern shocks. The only difference from the familiar shocks in non-porous materials is the compaction behavior reflected in the porous material's equation of state.

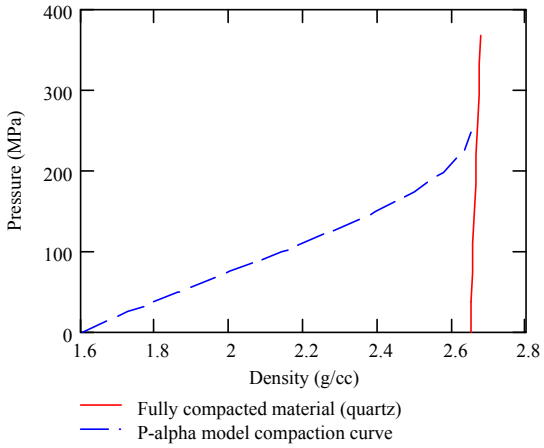

Fig. 1. The P-α model of sand compaction.

A pointy body thrust rapidly into a porous material drives the material aside and compacts it by a similar wave, which emanates at some angle from the penetrator apex. The angle depends on the apex angle, on whether the penetrator is a cone or wedge, and on the penetration velocity.

Relative to the penetrator, target material approaches at the penetration velocity U. This velocity is denoted V_1 and the velocity behind the shock V_2. The situation constitutes supersonic flow about an infinitely long wedge, as shown in Fig. 2. A particle approaching at velocity V_1 abruptly changes in velocity to V_2 in a direction parallel to the wedge's surface; thus it is deflected by an angle equal to the wedge's half-apex angle δ. The shock makes an angle σ with the flow direction.

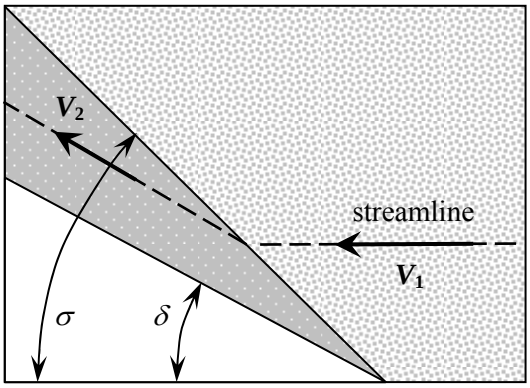

Fig. 2. Oblique compaction shock at a wedge.

The situation differs for a cone, Fig. 3. The angle δ by which the shock deflects the streamline is smaller than the apex angle β, and the flow behind the shock is nonuniform, as the streamline curves to asymptotically approach the cone angle and the sand undergoes further compaction.

Compaction Wave

The development and solution of the equations follows standard texts on gas dynamics (e.g., [3]). Changes in velocity, density, and pressure through the shock can be analyzed with the aid of Fig. 4, which shows velocity vectors before and behind the wave. Velocity components normal and transverse to the wave front are denoted by subscripts n and t.

The shock equations are:

Continuity in n-direction: $\rho_1 V_{1n} = \rho_2 V_{2n}$

Momentum in t-direction: $\rho_1 V_{1n} V_{1t} = \rho_2 V_{2n} V_{2t}$

Momentum in n-direction: $P_1 + \rho_1 V_{1n}^2 = P_2 + \rho_2 V_{2n}^2$

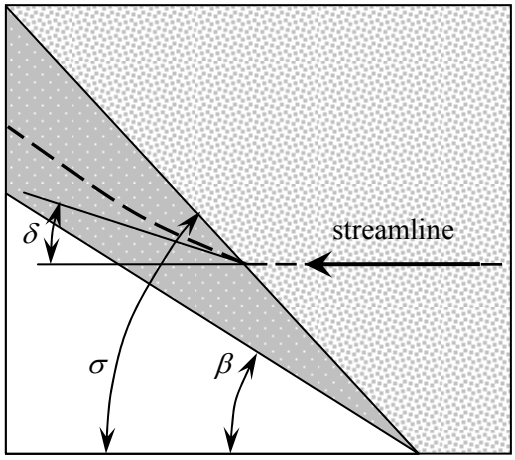

Fig. 3. Oblique compaction shock at a cone.

In terms of velocity magnitudes and angles, these equations may be written as:

$$\rho_1 V_1 \sin\sigma = \rho_2 V_2 \sin(\sigma - \delta) \tag{2}$$

$$\rho_1 V_1^2 \sin\sigma\cos\sigma = \rho_2 V_2^2 \sin(\sigma - \delta)\cos(\sigma - \delta) \tag{3}$$

$$P_1 + \rho_1 V_1^2 \sin^2\sigma = P_2 + \rho_2 V_2^2 \sin^2(\sigma - \delta) \tag{4}$$

to which is added the P-α model, applied to state 2 behind the shock,

$$\alpha_2 = \begin{cases} 1 + (\alpha_0 - 1)(1 - P_2/P_s)^2 & \text{for} \quad P_2 < P_s \\ 1 & \text{for} \quad P_2 \geq P_s \end{cases} \tag{5}$$

Equations (2-5) relate σ, ρ_2 (or α_2), V_2, P_2, and δ. For a wedge, the deflection angle δ is known, so a solution may be obtained. For a cone, however, the shock angle σ is treated as given and δ as unknown.

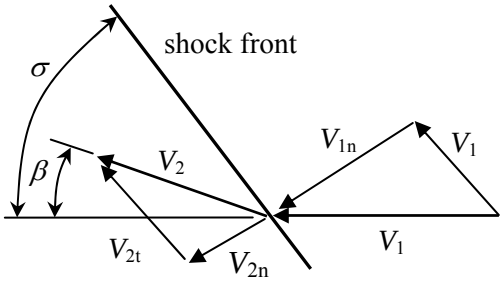

Fig. 4. Velocity changes across the oblique compaction wave.

Squaring Eq. (2) and dividing by Eq. (3) yields

$$\rho_1 \tan\sigma = \rho_2 \tan(\sigma - \delta) \tag{6}$$

Solving Eqs. (2) and (4) with $P_1 = 0$ yields

$$P_2 = \rho_1 V_1^2 \sin^2\sigma\left(1 - \rho_1/\rho_2\right) \tag{7}$$

For partial compaction in the shock ($P_2 < P_s$), Eqs. (5-7) can be combined into

$$\tan^3\sigma[(\alpha_0 - 1)(1 - B)^2 + 1]\tan\delta + \tan^2\sigma\left[\alpha_0 - 2B(\alpha_0 - 1)\right] + \tan\sigma\left[\alpha_0\tan\delta\right] + \alpha_0 = 0 \tag{8}$$

where $B \equiv \rho_1 V_1^2/P_s^2$. This equation, a cubic in $\tan\sigma$, is awkward; further, it is limited to partial compaction in the shock. It is easier to assume a value of σ, then solve for the other shock properties; this approach is sufficient to plot curves. By Eqs. (5) and (7),

$$\frac{\alpha_2 - 1}{\alpha_0 - 1} = \left[1 - B\sin^2\sigma\left(1 - \alpha_2/\alpha_0\right)\right]^2 \tag{9}$$

which, given σ, may be solved for the compaction parameter α_2,

$$\frac{\alpha_2}{\alpha_0} = 1 - \frac{1}{B^2\sin^4\sigma}\left[2B\sin^2\sigma - \frac{\alpha_0}{\alpha_0 - 1}\right] \tag{10}$$

Then

$$P_2 = \rho_1 V_1^2 \sin^2\sigma\left(1 - \alpha_2/\alpha_0\right) \tag{11}$$

$$\delta = \sigma - \arctan\left[(\alpha_2/\alpha_0)\tan\sigma\right] \tag{12}$$

$$V_2 = V_1 \frac{\sin\sigma}{\sin(\sigma - \delta)}\frac{\alpha_2}{\alpha_0} \tag{13}$$

The above development is based on partial compaction. As penetration velocity or shock angle increases, so does the shock pressure P_2, while α_2 decreases, eventually reaching a value of unity at complete compaction, for which $P_2 \geq P_s$, or, by Eq. (11),

$$\sin^2\sigma \geq \frac{\alpha_0}{\alpha_0 - 1}\frac{P_s}{\rho_1 V_1^2} \tag{14}$$

for complete compaction in the shock, $\alpha_2 = 1$. Equations (11-13) still hold, but Eq. (6) reduces to

$$\tan^2\sigma\tan\delta - \tan\sigma(\alpha_0 - 1) + \alpha_0\tan\delta = 0 \tag{15}$$

which has two roots

$$\tan\sigma = \frac{\alpha_0 - 1 \pm \sqrt{(\alpha_0 - 1)^2 - 4\alpha_0\tan^2\delta}}{2\tan\delta} \tag{16}$$

If the velocity is sufficient, the curve of σ vs. δ intersects this curve, then runs along it.

The relation between shock and deflection angles is shown in Fig. 5. The solid curve for complete compaction, Eq. (15), has for each δ two values of σ. For δ larger than about 14°, there is no solution, as an attached shock is not possible; here, any shock must be *detached* and stand as a bow shock ahead of the penetrator. Points on the curve's upper leg are not reachable; they correspond to the so-called "strong-shock" solution, but only the lower "weak-shock" value can occur.

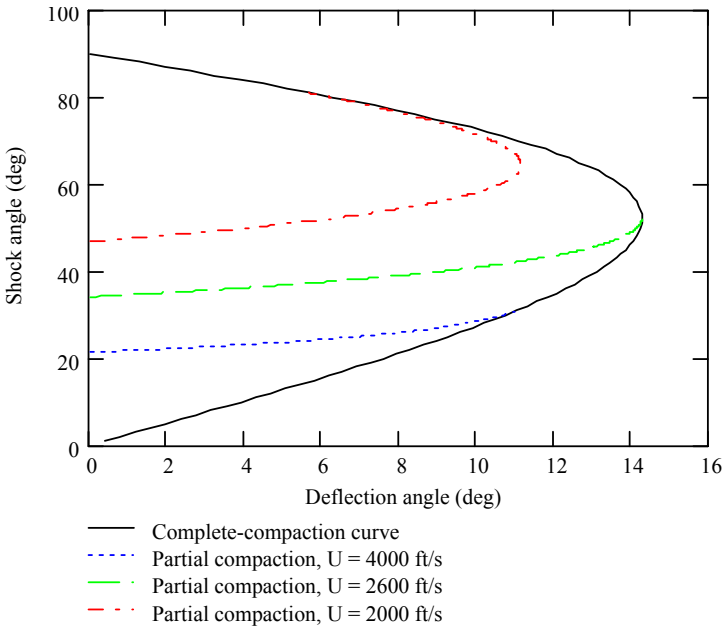

Fig. 5. Shock-deflection solutions for three velocities.

The other curves are partial-compaction curves for three penetration velocities. Of these, the dashed curve corresponds to a critical velocity, as it intersects the complete-compaction curve at its right end. This point is located by observing that Eq. (16) has a single value here, so the radicand must vanish, which yields the critical deflection δ_C,

$$\tan\delta_c = \frac{\alpha_0 - 1}{2\sqrt{\alpha_0}} \tag{17}$$

Substituting this into Eq. (16) yields

$$\tan\sigma_c = \sqrt{\alpha_0} \tag{18}$$

For $\alpha_0 = 1.655$, these formulas give $\delta_C = 14.3°$, $\sigma_C = 52.1°$, which is the rightmost point of the complete-compaction curve. Thus, for wedges blunter than 14.3° half-angle, an attached shock cannot exist, no matter how high the velocity.

The penetration velocity whose partial-compaction σ-δ curve intersects the complete-compaction curve at this point corresponds to $P_2 = P_s$, $\alpha_2 = 1$, and $\sigma = \sigma_C$, for which Eq. (11) gives the velocity

$$U_c = \sqrt{\frac{P_s}{\rho_1}\frac{\alpha_0 + 1}{\alpha_0 - 1}} \tag{19}$$

At velocities above this, complete compaction occurs in the shock for deflection angles greater than a certain value. For the P-α model, this critical velocity is about 2600 ft/s.

The dash-dot curve in Fig. 5 is the partial-compaction curve for a velocity, 2000 ft/s, below this critical value. It intersects the complete-compaction curve on its unreachable upper leg. At such sub-critical velocities, complete compaction cannot occur in the shock. Note that this curve's rightmost point lies left of the rightmost point of the full-compaction curve; for deflection angles greater than this point's, an attached shock is not possible, and any shock must be detached. The maximum deflection angle is given by Eq. (8) with $\partial\delta/\partial\sigma = 0$, or equivalently by $\partial(\tan\delta)/\partial(\tan\sigma) = 0$, which yields the condition

$$3\tan^2\sigma_{max}\,\tan\delta_{max}[(\alpha_0 - 1)(1 - B)^2 + 1] - 2\tan\sigma_{max}\left[2B(\alpha_0 - 1) - \alpha_0\right] + \alpha_0\tan\delta_{max} = 0$$

which in conjunction with Eq. (8) locates the point of maximum deflection for a given velocity. Eliminating tan δ_{max} from these two equations yields

$$AC\tan^4\sigma_{max} - \tan^2\sigma_{max}(C+3A)\alpha_0 + \alpha_0^2 = 0$$

where $A \equiv (\alpha_0 - 1)(1-B)^2 + 1$ and $C \equiv 2B(\alpha_0 - 1) - \alpha_0$, for which the solution is

$$\tan^2\sigma_{max} = \alpha_0 \frac{C + 3A + \sqrt{(C+3A)^2 + 4AC}}{2AC} \tag{20}$$

The maximum deflection angle for an attached shock is then given by

$$\tan\delta_{max} = \frac{2[2B(\alpha_0 - 1) - \alpha_0]\tan\sigma_{max}}{3[(\alpha_0 - 1)(1-B)^2 + 1]\tan^2\sigma_{max} + \alpha_0} \tag{21}$$

For a penetration velocity of 2000 ft/s, this angle is about 11°.

The dotted line in Fig. 5 is the partial-compaction curve for a velocity, 4000 ft/s, above that given by Eq. (19). It intersects the complete-compaction curve along its lower leg, at a deflection angle of about 11°. For deflection angles smaller than this, only partial compaction occurs in the shock; for larger deflections, complete compaction occurs there.

Each partial-compaction curve in Fig. 5 meets the vertical axis at a positive value, the minimum possible shock angle, which corresponds to an infinitesimal deflection or a shock of vanishing strength traveling at the sound speed $c_0 = \sqrt{dP/d\rho}$. Differentiating Eq. (1) and evaluating at $\alpha = \alpha_0$ yields $c_0^2 = \alpha_0 P_s/[2\rho_0(\alpha_0 - 1)]$. For $\alpha_0 = 1.66$, $P_s = 250$ MPa, $\rho_0 = 1.6$ g/cm^3, the sound speed is 443 m/s. The minimum shock angle is the Mach angle, $\sin^{-1}(c_0/U)$.

This model requires an attached shock, whose existence depends on the velocity and deflection angle. At velocities below the sound speed c_0, no shock is possible. At velocities above the critical value U_c of Eq. (19), the shock is attached for deflection angles up to δ_C of Eq. (17). Between c_0 and U_c, the shock is attached for deflection angles up to δ_{max} given by Eq. (21).

Curves for these equations divide the plane of velocity vs. deflection angle in Fig. 6 and define the limits of applicability of the attached-shock model. The model holds at all points above the dashed curve, which corresponds to Eqs. (20-21); below, the shock is detached or non-existent (in the sub-

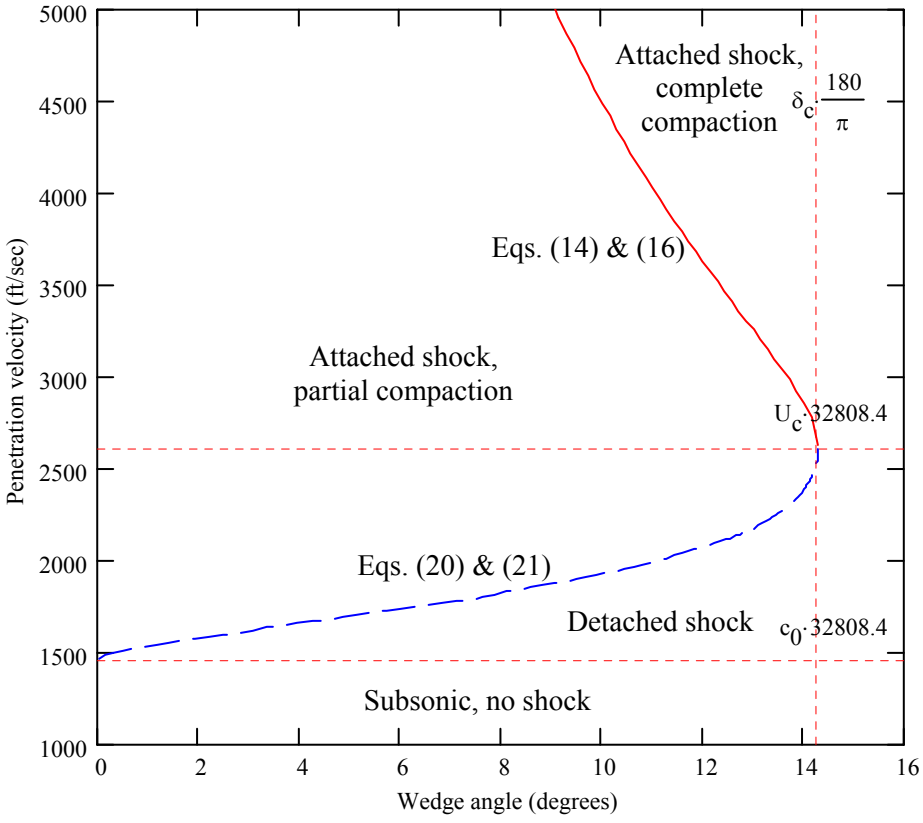

Fig. 6. Regimes of shock behavior over the plane of penetration velocity vs. shock deflection angle.

sonic regime at the bottom). Above the solid curve of Eqs. (14) and (16), the shock completely compacts the sand. Between these curves, the shock only partially compacts the sand.

Conical Flow Behind the Shock

A conical penetrator differs from a wedge in that the flow is axisymmetric, and behind the shock, as in Fig. 3, each streamline curves as it approaches the cone. This flow is determined from the solution of Taylor and Maccoll[4] for supersonic flow about a cone. The same dynamical equations are used here, but the P-α model replaces the ideal gas law.

The solution is based on the observation that, for flow about a cone of infinite extent, the problem involves no length dimension; the solution therefore depends only on angles centered on the cone's apex. Using a spherical coordinate system centered here reduces the equations for the flow behind the shock to the ordinary differential equations,

$$2V_r + V_\theta \cot\theta + \left[\frac{dV_\theta}{d\theta} - \frac{V_\theta}{\alpha}\frac{d\alpha}{d\theta}\right] = 0\,;\; V_\theta = dV_r/d\theta\,;\; \frac{dP}{d\theta} = -\frac{\rho_s}{\alpha}\left[V_r\frac{dV_r}{d\theta} + V_\theta\frac{dV_\theta}{d\theta}\right] \quad (22)$$

where V_r and V_θ are velocity components in the radial and angular directions (measured from the apex). The boundary conditions are the states behind the shock given by the oblique-shock relations, and $V_\theta = 0$ at the cone's surface.

The solution scheme is inverse. For a given U, a value of shock angle σ is assumed. The conditions behind the shock are given by Eqs. (10-13). Velocity components there are given by $V_\theta\big|_{\theta=\sigma} = V_2 \sin(\sigma - \delta)$; $V_r\big|_{\theta=\sigma} = V_2 \cos(\sigma - \delta)$. Eqs. (22) are then numerically integrated from the shock to the cone for decreasing θ, until $V_\theta = 0$, which satisfies the boundary condition at the surface, where the value of θ is the apex angle β that yields this solution. At low velocities, the sand is only partially compacted, but at increasing velocities, complete compaction occurs first near the cone surface, then encompasses an increasing angle, until complete compaction occurs in the shock.

Calculated results at 3000 ft/s are shown in Fig. 7, which plots the relationships among the various angles. The dark-blue curve relates shock angle to deflection angle at full compaction. The green curve intersecting the vertical axis at the Mach angle of 29.1° relates the shock and deflection angles; it starts to overwrite the blue curve at a shock angle of 43.4°, where full compaction in the shock begins. Its right end corresponds to the

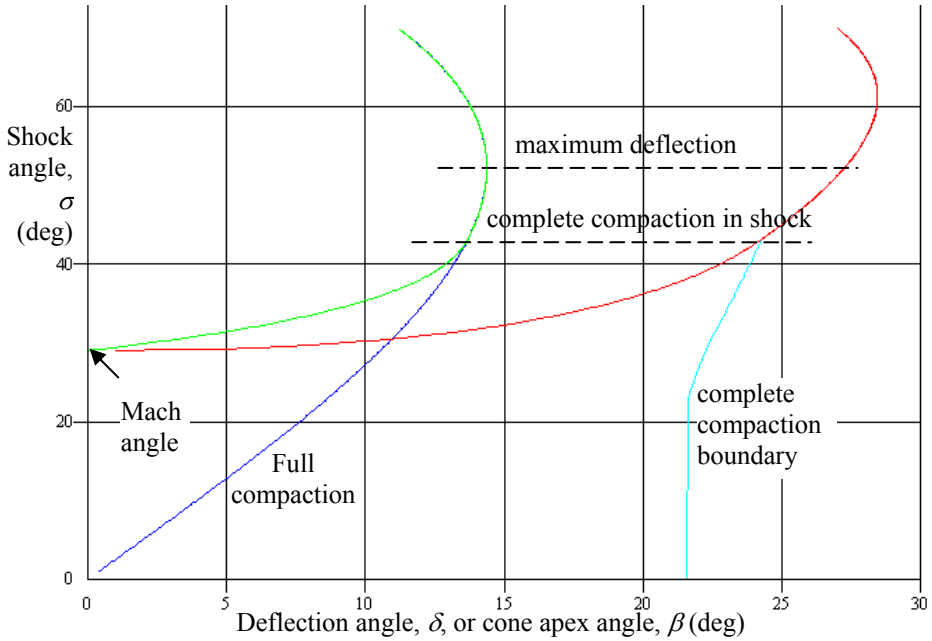

Fig. 7. Computed results for a penetration velocity of 3,000 ft/s.

maximum deflection for an attached shock, 14.3°, at a shock angle of 52.2°. The red curve relates shock angle to cone apex angle; because the maximum shock angle is 52.2° (upper dashed line), the uppermost point reachable on this curve is at an apex angle of 27.2°. The light-blue curve locates the boundary between partially and fully compacted sand; for apex angles less than about 22°, no sand is fully compacted, but as β increases, this boundary expands outward from the cone surface until full compaction occurs in the shock, where it intersects the shock-angle curve (lower dashed line) at about a 24° apex.

COMPARISON WITH HYDROCODE

To compare with the model, the CTH hydrocode[5] was run for cones penetrating dry sand modeled by the *P*-α model. Figure 8 shows the result for a 20° cone at 3,000 ft/s. The plot, of color contours of density, reveals an oblique wave (in green) attached to the apex of the (red) cone. The model predicts a shock angle of about 36.1°, in good agreement with the angle in this plot (35.5°).

Computations were run for apex angles of 10° to 30° and velocities of 3,000 and 4,000 ft/s. Values of shock angle σ measured from the CTH plots are compared with model predictions in Table 1; agreement is within a fraction of a degree in all but one case. For the 30° cone, the model predicts detached shocks at both velocities, and the CTH plots, as in Fig. 9, clearly show curved waves. The CTH values are shown on the model plots in Fig. 10.

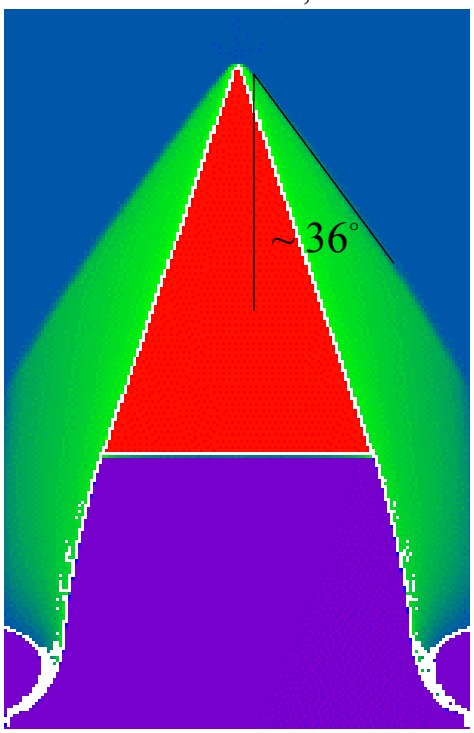

Fig. 8. CTH computation of a 20° cone penetrating sand at 3,000 ft/s.

Table 1. Comparison of analytical model and CTH computations for conical penetrators.

Half-apex angle, β	Shock angle, σ			
	U = 3,000 ft/s		U = 4,000 ft/s	
	Model	CTH	Model	CTH
10°	30.2°	30.5°	22.9°	22.4°
15°	32.3°	32.8°	26.1°	26.6°
20°	36.1°	35.5°	33.8°	34.3°
25°	45.0°	45.0°	45.0°	43.3°
30°	detached	curved	detached	curved

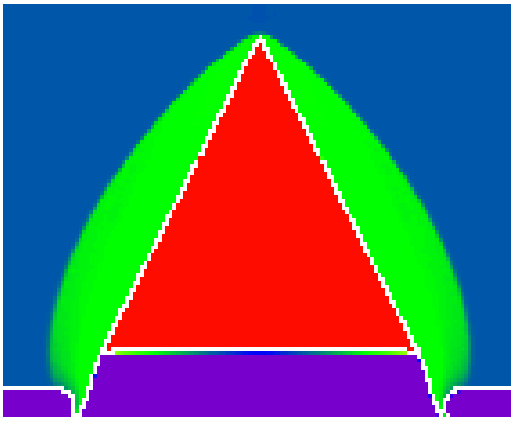
Fig. 9. CTH computation of a 30°-half-angle cone penetrating dry sand at 3,000 ft/s.

CONCLUSIONS

An analytical model for pointy wedges and cones penetrating dry sand at supersonic velocities has been developed. The model predicts the pressure acting on the penetrator. Agreement with hydrocode computations is excellent.

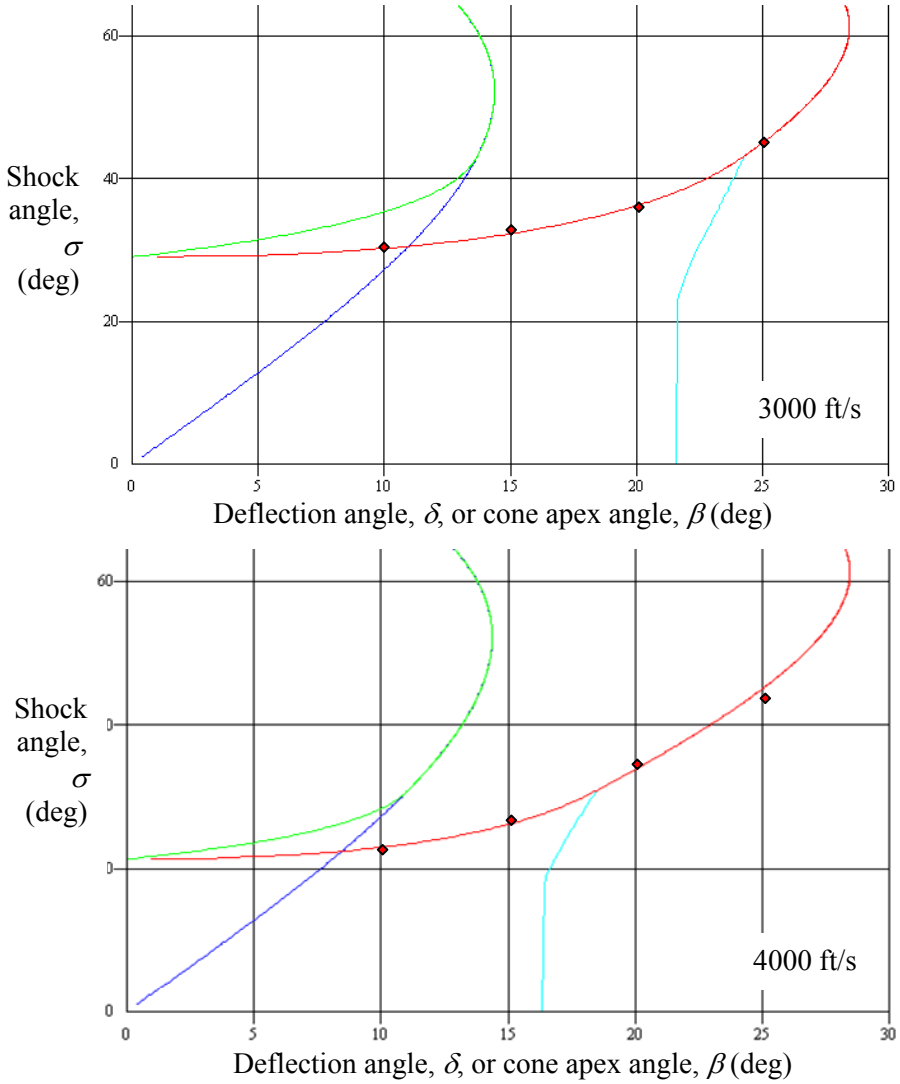

Fig. 10. Model solutions (curves) and CTH predictions (symbols) of shock angle for penetration at 3,000 ft/s (top) and 4,000 ft/s (bottom).

ACKNOWLEDGMENT

The support of the U.S. Air Force Research Laboratory is gratefully acknowledged.

REFERENCES

1. W. Herrmann, *J. Appl. Phys.*, vol. 40, pp. 2490-2499, 1969.
2. G. Kerley, "The Effects of Soil Type on Numerical Simulations of Buried Mine Explosions," Kerley Technical Services, KTS02-3, August 2002.
3. J.D. Anderson, Jr., *Modern Compressible Flow*, 2nd ed., McGraw-Hill, New York, 1990.
4. G.I. Taylor and J.W. Maccoll, "The Air Pressure on a Cone Moving at High Speed," *Proc. Roy. Soc. (London)*, ser. A, vol. 139, 1933.
5. E.S. Hertel et al., "CTH: A Software Family for Multi-Dimensional Shock Physics Analysis," *Proc. 19th Intl. Symp. Shock Waves*, Vol. 1, pages 377-382, Marseilles, France, 26-30 July 1993.